



THE UNIVERSITY *of* EDINBURGH

## Edinburgh Research Explorer

### **Ca<sup>2+</sup> activity signatures of myelin sheath formation and growth in vivo**

**Citation for published version:**

Baraban, M, Koudelka, S & Lyons, DA 2018, 'Ca<sup>2+</sup> activity signatures of myelin sheath formation and growth in vivo', *Nature Neuroscience*, vol. 21, no. 1, pp. 19–23. <https://doi.org/10.1038/s41593-017-0040-x>

**Digital Object Identifier (DOI):**

[10.1038/s41593-017-0040-x](https://doi.org/10.1038/s41593-017-0040-x)

**Link:**

[Link to publication record in Edinburgh Research Explorer](#)

**Document Version:**

Peer reviewed version

**Published In:**

Nature Neuroscience

**General rights**

Copyright for the publications made accessible via the Edinburgh Research Explorer is retained by the author(s) and / or other copyright owners and it is a condition of accessing these publications that users recognise and abide by the legal requirements associated with these rights.

**Take down policy**

The University of Edinburgh has made every reasonable effort to ensure that Edinburgh Research Explorer content complies with UK legislation. If you believe that the public display of this file breaches copyright please contact [openaccess@ed.ac.uk](mailto:openaccess@ed.ac.uk) providing details, and we will remove access to the work immediately and investigate your claim.



1 **Ca<sup>2+</sup> activity signatures of myelin sheath formation and growth *in vivo***

2  
3  
4

5 Marion Baraban<sup>1</sup>, Sigrid Koudelka<sup>1</sup> and David A Lyons<sup>1</sup>.

6  
7  
8  
9

10 1. Centre for Neuroregeneration, Centre for Discovery Brain Sciences, University of Edinburgh, 49 Little  
11 France Crescent, Edinburgh EH16 4SB, UK.

12  
13  
14

15 Correspondence prior to publication to David A Lyons (david.lyons@ed.ac.uk) and after publication to  
16 either David A Lyons or Marion Baraban (marion.baraban@ed.ac.uk)

17  
18  
19

20 During myelination, individual oligodendrocytes initially over-produce short myelin sheaths that are  
21 either retracted or stabilised. By live imaging oligodendrocyte  $\text{Ca}^{2+}$  activity *in vivo*, we find that high-  
22 amplitude long-duration  $\text{Ca}^{2+}$  transients in sheaths prefigure retractions, mediated by calpain.  
23 Following stabilisation, myelin sheaths grow along axons, and we find that higher frequency  $\text{Ca}^{2+}$   
24 transient activity in sheaths precedes faster elongation. Our data implicate local  $\text{Ca}^{2+}$  signalling in  
25 regulating distinct stages of myelination.

26

27

28 Dynamic regulation of myelination by oligodendrocytes in the central nervous system (CNS) is essential  
29 for nervous system development and life-long function<sup>1</sup>, but our understanding of myelin sheath  
30 formation and growth is limited. Zebrafish are well suited to studying the dynamics of CNS myelination  
31 *in vivo*, due to their capacity for non-invasive longitudinal imaging. Previous imaging studies using  
32 zebrafish have shown that individual oligodendrocytes initiate formation and elongation of their  
33 myelin sheaths within a critical period of about 5 hours<sup>2,3</sup>, mirroring hours-long myelin sheath  
34 generation by mammalian oligodendrocytes *in vitro*<sup>4</sup>. During sheath formation, myelinating  
35 oligodendrocytes initially overproduce short myelin sheaths (circa 5  $\mu\text{m}$  in length), with some stabilised,  
36 and others fully retracted<sup>2,3,5,6</sup>. Following stabilisation, myelin sheaths grow along and around  
37 associated axons<sup>3</sup>, to achieve dimensions that mediate the timing of impulse conduction and thus  
38 neural circuit function<sup>7</sup>. Although axonal signals, including neuronal activity, can regulate the formation  
39 and growth of myelin sheaths (e.g.<sup>5,8-10</sup>), the localised signalling mechanisms that control the dynamics  
40 of myelination by oligodendrocytes remain to be elucidated.

41  $\text{Ca}^{2+}$  is a second messenger that regulates many events, and localised  $\text{Ca}^{2+}$  activity has been observed  
42 in oligodendrocyte precursor cells<sup>11</sup>, myelinating oligodendrocytes<sup>10</sup>, and even in mature myelin  
43 sheaths<sup>12</sup> *in vitro* and *ex vivo*. We reasoned that determining how localised  $\text{Ca}^{2+}$  activity relates to the  
44 formation and growth of myelin sheaths *in vivo* would provide novel insights into mechanisms of CNS  
45 myelination.

46

47

48 To visualise  $\text{Ca}^{2+}$  activity in myelinating oligodendrocytes, we used the genetically encoded calcium  
49 indicator GCaMP6s<sup>13</sup>, which we expressed in oligodendrocytes by crossing Tg(sox10:KaITa4) and  
50 Tg(uas:GCaMP6s) transgenic zebrafish lines (Online Methods). We imaged GCaMP6s expressing  
51 oligodendrocytes in the spinal cord of zebrafish larvae between 3-4 days post fertilisation (dpf), as  
52 myelin sheaths are being formed and starting to elongate<sup>2,3</sup>. We first assessed the kinetics of individual

53 localised  $\text{Ca}^{2+}$  transients in myelin sheaths by high-speed 2D (4Hz) imaging, and found that essentially  
54 all transients lasted longer than 3.5 seconds (Supplementary Fig. 1, Supplementary Movie 1).  
55 Therefore, we 3D imaged  $\text{Ca}^{2+}$  activity in all myelin sheaths belonging to individual oligodendrocytes  
56 with a time interval of 2.5 seconds (Fig. 1A-E, Online Methods, Supplementary Fig. 2, and  
57 Supplementary Movies 2 and 3).

58

59 To correlate  $\text{Ca}^{2+}$  activity with myelination, we time-lapse imaged individual GCaMP6s-expressing  
60 oligodendrocytes for multiple 20 minute blocks over a 5-9 hour period during which they initiated  
61 formation and elongation of their myelin sheaths (Fig. 1F,G). Prior to each  $\text{Ca}^{2+}$  imaging block, we  
62 acquired a high-resolution 3D z-stack of GCaMP6s-expressing oligodendrocytes together with  
63 *sox10:mRFP*, which allowed assessment of sheath morphology (Fig. 1F,G and see Online Methods). We  
64 quantified the  $\text{Ca}^{2+}$  activity of 305 sheaths of 18 oligodendrocytes in 18 animals. Analyses of 448  $\text{Ca}^{2+}$   
65 transients in the 187 sheaths that exhibited activity (out of the 305 sheaths imaged) revealed significant  
66 diversity in the frequency (Fig.1H), amplitude and duration of transients between sheaths (Fig. 1I,J)  
67 (Median amplitude per sheath  $\Delta F/F_0 = 0.7$ , IQR=0.9; Median  $\text{Ca}^{2+}$  transient duration= 23s, IQR=17  
68 seconds per sheath). We also found that duration and amplitude were positively correlated, whereby  
69 longer duration transients tended to also be of higher amplitude (Fig. 1K).

70

71 The diversity in  $\text{Ca}^{2+}$  transient activity between sheaths suggested that their frequency, duration and/or  
72 amplitude may influence myelination. We first focussed on the relationship between  $\text{Ca}^{2+}$  activity and  
73 myelin sheath formation. We found that 61 of the 305 sheaths analysed were completely retracted  
74 during our imaging protocol, reflecting the initial over-production of sheaths. Intriguingly, we found  
75 that the amplitude of  $\text{Ca}^{2+}$  transients in sheaths that were subsequently retracted was three-fold higher  
76 than in those sheaths that were stabilised (Fig. 2A,B,D: Median amplitude =1.8  $\Delta F/F_0$  in fully retracted  
77 sheaths vs 0.6  $\Delta F/F_0$  in stabilised sheaths). Furthermore, we observed an increase in  $\text{Ca}^{2+}$  transient  
78 duration in sheaths that were subsequently retracted (Fig.2C,D: Median duration= 35s in retracted  
79 sheaths vs 22s in stabilised). Interestingly, the  $\text{Ca}^{2+}$  transients observed in sheaths that were  
80 subsequently retracted travelled from sheath to process (Supplementary Fig. 3, Supplementary Movie  
81 4), reflecting the directionality of retraction, first of the sheath and then the process (Fig. 2A,  
82 Supplementary Fig. 4). These observations lead us to hypothesise that localised high-amplitude long-  
83 duration  $\text{Ca}^{2+}$  transients may mediate sheath retraction through activation of  $\text{Ca}^{2+}$ -dependent  
84 mechanisms.

85

86 We hypothesised that calpain enzymes,  $\text{Ca}^{2+}$  dependent non-lysosomal proteases, might mediate  
87 sheath retraction. Calpains underpin many aspects of cellular breakdown, including the localised  
88 pruning of dendrites in *Drosophila* following large  $\text{Ca}^{2+}$  transients<sup>14</sup>. To test whether calpain mediates  
89 myelin sheath retractions, we took chemical and genetic approaches. We first treated animals with the  
90 calpain inhibitor PD150606<sup>15</sup> from 2-4 dpf, and assessed the morphology of individual  
91 oligodendrocytes with mbp:mCherry-CAAX<sup>6</sup>. We found that PD150606 treatment increased myelin  
92 sheath number per oligodendrocyte (Fig. 2E,H) (Average sheath number per oligodendrocyte: DMSO  
93  $14.4 \pm 3.2$  vs PD150606  $18.7 \pm 5.9$ ). In order to whether calpain actually mediates retraction of sheaths,  
94 we carried out time-lapse microscopy of PD150606-treated animals. These studies revealed a lower  
95 rate of sheath retraction in calpain-inhibited animals during the dynamic period of sheath stabilisation  
96 and retraction (Fig. 2F,I and Supplementary movies 5+6) (Sheath retraction per oligodendrocyte per  
97 hour, DMSO  $0.34 \pm 0.13$  vs PD150606  $0.24 \pm 0.13$ ). To independently and cell autonomously test the role  
98 for calpain in regulating myelin sheath number, we expressed the endogenous inhibitor of calpain,  
99 calpastatin<sup>16</sup>, in myelinating oligodendrocytes (see Online Methods and Supplementary Fig. 5). Analysis  
100 of oligodendrocyte morphology revealed that cell-type specific disruption of calpain protease function  
101 increased the number of myelin sheaths compared to control (Fig. 2G,J) (Average sheath number per  
102 cell mbp:meGFP  $15.8 \pm 6.4$  vs mbp:meGFP-calpastatin  $20.5 \pm 5.8$ ).  
103 Together, these data support our imaging-driven hypothesis that calpain regulates retraction of myelin  
104 sheaths during the dynamic period of myelin sheath formation by individual oligodendrocytes.

105

106 We next assessed how  $\text{Ca}^{2+}$  transient activity might relate to myelin sheath growth. By comparing  $\text{Ca}^{2+}$   
107 activity and differential growth over time (Fig. 3A,B), we found that the frequency of the lower  
108 amplitude shorter duration  $\text{Ca}^{2+}$  transients observed in stabilised sheaths correlated positively with the  
109 speed of sheath elongation (Fig. 3C,D). Interestingly, when we analysed how individual sheaths grew  
110 after each  $\text{Ca}^{2+}$  transient, we observed positive elongation within the first 2 hours of the  $\text{Ca}^{2+}$  transient  
111 (Fig. 3E). We did not see any correlation between the average amplitude or duration of transients with  
112 the speed of growth (Supplementary Fig. 6). These observations show the frequency of low amplitude  
113 short duration  $\text{Ca}^{2+}$  transients in stabilised sheaths is predictive of their speed of elongation, suggesting  
114 that dynamic changes in myelin sheath  $\text{Ca}^{2+}$  concentration regulate sheath growth.

115

116 Our live imaging has revealed distinct signatures of localised  $\text{Ca}^{2+}$  activity during CNS myelination. High-  
117 amplitude long duration  $\text{Ca}^{2+}$  transients precede localised retraction of sheaths, mediated by calpain,  
118 whereas the frequency of lower amplitude shorter duration transients in stabilised sheaths correlates

119 positively with their speed of elongation (Summarised in Supplementary Fig. 7). How could distinct  $\text{Ca}^{2+}$   
120 signatures lead to such different outcomes during myelination? With respect to sheath retraction, it is  
121 known that different isoforms of calpain have distinct sensitivities to  $\text{Ca}^{2+}$  concentration, with some  
122 primed for activation by localised changes in  $\text{Ca}^{2+}$  concentration<sup>17</sup>. It is possible that large localised  
123 increases in  $\text{Ca}^{2+}$  concentration following individual high-amplitude long-duration transients could  
124 stimulate local protease activity that leads to sheath retraction, e.g. by localised degradation of  
125 cytoskeletal components. With respect to the speed of sheath elongation, it is now known that myelin  
126 sheath growth occurs is driven at inside of the myelin sheath<sup>3</sup>, at least in part, by iterative cycles of  
127 actin polymerisation and depolymerisation<sup>18</sup>. Given that actin polymerisation/depolymerisation can be  
128 regulated by  $\text{Ca}^{2+}$ , it is possible that localised changes in  $\text{Ca}^{2+}$  concentration could affect the speed of  
129 sheath growth via regulating the actin cytoskeleton.

130

131 Many additional questions remain as to how localised  $\text{Ca}^{2+}$  regulates myelination. Which signal(s) lead  
132 to the distinct changes in myelin sheath  $\text{Ca}^{2+}$  during retraction, stabilisation and growth? Neuronal  
133 activity is one signal known to affect myelination<sup>5,8-10</sup>, and many of its candidate mediators in  
134 oligodendrocytes converge on regulation of intracellular  $\text{Ca}^{2+}$ <sup>19</sup>. Indeed, a complementary study to  
135 ours indicates that neuronal activity regulates about half of the  $\text{Ca}^{2+}$  transients in myelin<sup>20</sup>. How  $\text{Ca}^{2+}$   
136 might affect ongoing sheath growth and remodelling throughout life, and during regeneration, also  
137 remain to be investigated. We anticipate that live  $\text{Ca}^{2+}$  imaging-focussed approaches will continue to  
138 elucidate the mechanisms underlying the dynamic regulation of myelination in the CNS.

139

#### 140 **Accession codes**

141 The Genbank accession number for *calpastatin* mRNA is MG387170.

142

#### 143 **Author contributions**

144 MB designed and performed experiments and co-wrote manuscript. SK performed experiments using  
145 chemical inhibitors. DAL designed experiments, managed project and co-wrote manuscript.

146

#### 147 **Acknowledgements**

148 We would like to thank members of the Lyons lab, as well as Thomas Becker, Peter Brophy, Charles  
149 ffrench-Constant, Matthew Livesey, Dies Meijer, Will Talbot and Claire Wyart for helpful comments on  
150 the manuscript. We would like to thank Herwig Baier for transgenic zebrafish, Bertrand Vernay for

151 support in image analysis. This work was supported by a Lister Institute Research Prize and a Wellcome  
152 Trust Senior Research Fellowship (102836/Z/13/Z) to DAL.

153

154 **Competing financial interests**

155 I declare that the authors have no competing interests as defined by Springer Nature, or other interests  
156 that might be perceived to influence the results and/or discussion reported in this paper.

157

158

159 **References**

160 1. Chang, K.-J., Redmond, S.A. & Chan, J.R. *Nat Neurosci* **19**, 190–197 (2016).  
161 2. Czopka, T., Ffrench-Constant, C. & Lyons, D.A. *Developmental Cell* **25**, 599–609 (2013).  
162 3. Snaidero, N. et al. *Cell* **156**, 277–290 (2014).  
163 4. Watkins, T.A., Emery, B., Mulinyawe, S. & Barres, B.A. *Neuron* **60**, 555–569 (2008).  
164 5. Hines, J.H., Ravanelli, A.M., Schwindt, R., Scott, E.K. & Appel, B. *Nat Neurosci* **18**, 683–689  
165 (2015).  
166 6. Mensch, S. et al. *Nat Neurosci* **18**, 628–630 (2015).  
167 7. Fields, R.D. *Nat Rev Neurosci* **16**, 756–767 (2015).  
168 8. Wake, H. et al. *Nature Communications* **6**, 7844 (2015).  
169 9. Koudelka, S. et al. *Curr. Biol.* **26**, 1447–1455 (2016).  
170 10. Wake, H., Lee, P.R. & Fields, R.D. *Science* **333**, 1647–1651 (2011).  
171 11. Sun, W., Matthews, E.A., Nicolas, V., Schoch, S. & Dietrich, D. *Elife* **5**, (2016).  
172 12. Micu, I. et al. *Experimental Neurology* **276**, 41–50 (2016).  
173 13. Chen, T.-W. et al. *Nature* **499**, 295–300 (2013).  
174 14. Kanamori, T. et al. *Science* **340**, 1475–1478 (2013).  
175 15. Wang, K.K. et al. *PNAS* **93**, 6687–6692 (1996).  
176 16. Moldoveanu, T., Gehring, K. & Green, D.R. *Nature* **456**, 404–408 (2008).  
177 17. Campbell, R.L. & Davies, P.L. *Biochem. J.* **447**, 335–351 (2012).  
178 18. Nawaz, S. et al. *Developmental Cell* **34**, 139–151 (2015).  
179 19. Pitman, K.A. & Young, K.M. *Int. J. Biochem. Cell Biol.* **77**, 30–34 (2016).

180 20

181

182

183

184

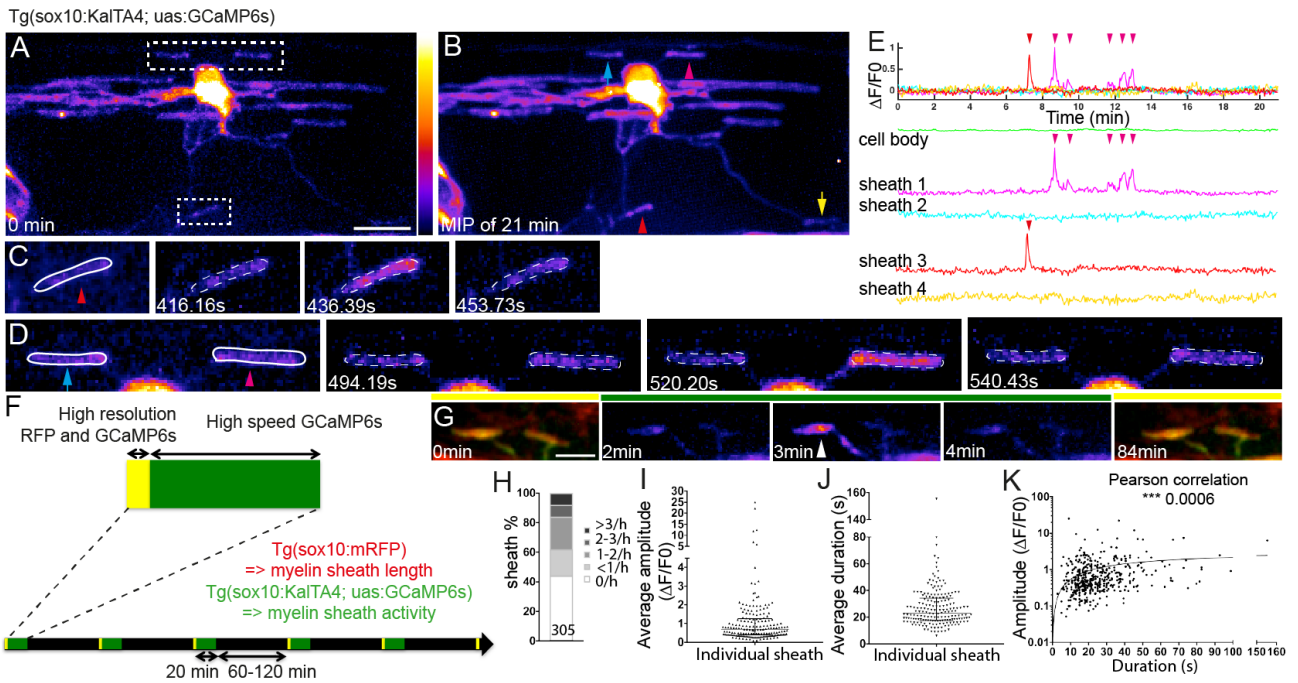


**Figure 1. Live imaging reveals localised  $\text{Ca}^{2+}$  activity in newly forming myelin sheaths**

A. Maximum intensity projection of a 3D z-stack of the first time-point from a 21 minute-long movie of a GCaMP6s expressing oligodendrocyte. Two areas of interest indicated, top corresponding to D and bottom to C. Scale bar= 10 $\mu\text{m}$ . Fire LookUpTable.

B. Maximum intensity projection of all time-points of cell shown in A. Arrowheads indicate sheaths with increased fluorescence, reflecting  $\text{Ca}^{2+}$  activity during the movie. Arrows point to sheaths with no increase.

C, D, myelin sheaths demarcated within ROIs outlined in A, at indicated times.

E.  $\Delta F/F_0$  over time. Arrowheads indicate sheaths shown in corresponding colours in B, C and D.

F. Schematic of time-lapse imaging experiment with interspersed imaging of cell morphology (yellow) and  $\text{Ca}^{2+}$  (green).

G. Sample images of myelin sheath morphology (under yellow bars) with intervening periods of  $\text{Ca}^{2+}$  imaging (under green bar). Arrowhead points to  $\text{Ca}^{2+}$  transient in sheath. Scale bar=5 $\mu\text{m}$ .

H. Distribution of  $\text{Ca}^{2+}$  transient frequencies of 305 sheaths, analysed in 18 animals.

I. Distribution of average  $\text{Ca}^{2+}$  transient amplitude per sheath (187 sheaths from 18 animals). Graph shows median and 1<sup>st</sup> and 3<sup>rd</sup> quartiles.

J. Distribution of average  $\text{Ca}^{2+}$  transient duration per sheath (187 sheaths from 18 animals). Graph shows median and 1<sup>st</sup> and 3<sup>rd</sup> quartiles.

K. Correlation between amplitude and duration per individual  $\text{Ca}^{2+}$  transient events (448 events from 187 sheaths in 18 animals, Pearson's Correlation Test,  $p=0.0006$ ).



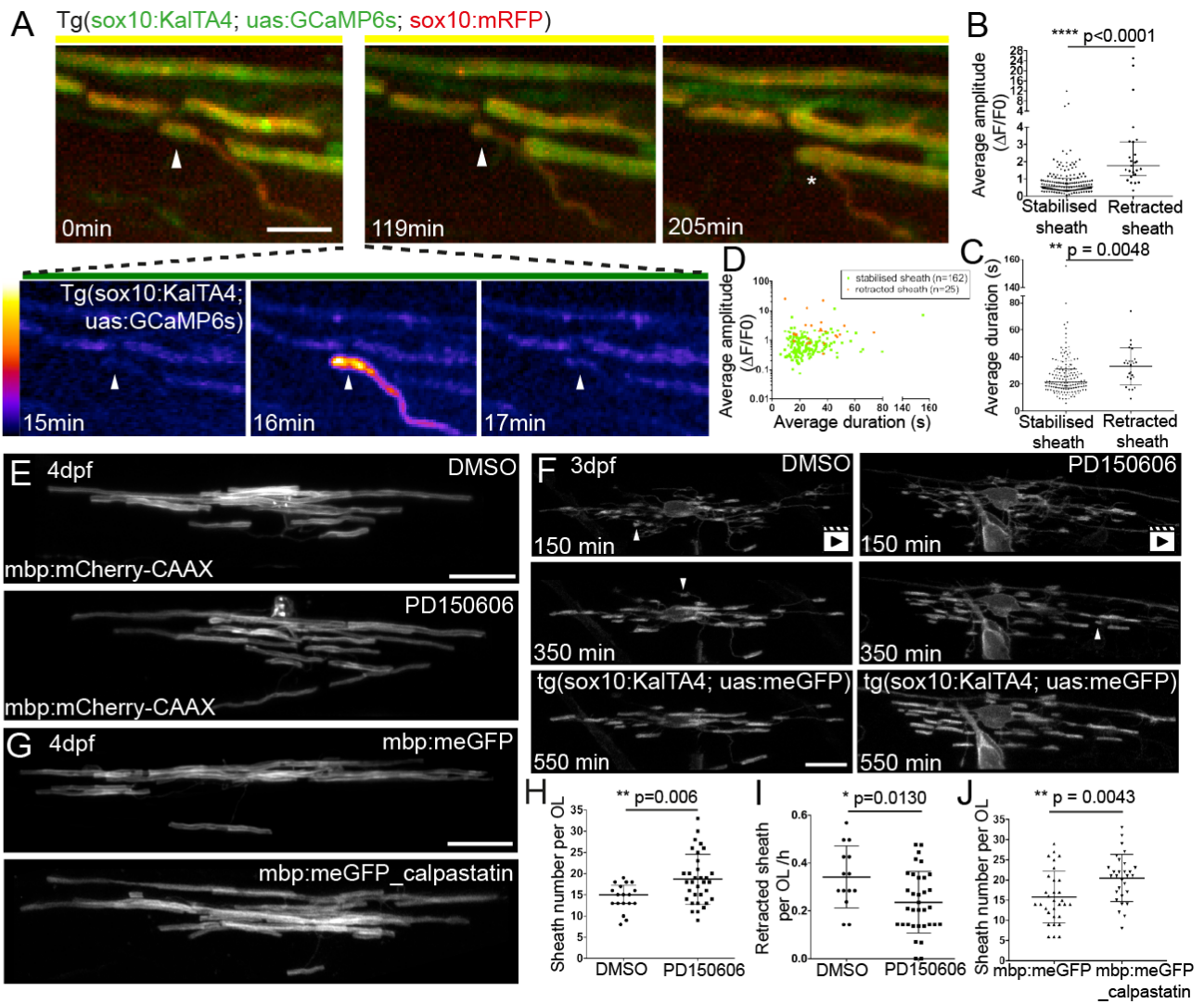


**Figure 2. High-amplitude long duration  $\text{Ca}^{2+}$  transients precede calpain-driven sheath retractions.**

A. Frames from a time-lapse imaging experiment. The myelin sheath imaged in high-resolution mode (0 min) exhibits a  $\text{Ca}^{2+}$  transient 16 minutes into a period of high-speed GCaMP6s imaging (see also Supplementary Fig. 3) subsequently retracts, first along the length of the axon (119 min) and then entirely from the axon (205 min, asterisk). Scale bar= 5 $\mu\text{m}$ .

B. Average amplitude of  $\text{Ca}^{2+}$  transients in sheaths that are either stabilised or fully retracted (n=25 retracted sheaths, 12 animals and n=162 stabilised sheaths, 18 animals; Graph shows median and 1<sup>st</sup> and 3<sup>rd</sup> quartiles. Two-tailed Mann-Whitney test,  $p < 0.0001$ .

C. Average duration of  $\text{Ca}^{2+}$  transients in sheaths shown in B. Graph shows median and 1<sup>st</sup> and 3<sup>rd</sup> quartiles. Two-tailed Mann-Whitney test,  $p = 0.0048$ .

D. Average amplitude and average duration of transient events in sheaths that are stabilised (green) or fully retracted (orange).

E. mbp:mCherry-CAAX expressing oligodendrocytes in control (top) and PD150606 treated animal (bottom) at 4 dpf. Scale bar= 10 $\mu\text{m}$ . Quantitation in 2H.

222 F. Frames from time-lapse movies of oligodendrocytes during myelination in a DMSO treated (left) and  
223 PD150606 treated (right) animal. Arrowheads point to sheaths that are retracted. See also  
224 Supplementary Movies 5+6. Scale bar= 10µm. Quantitation in 2I.

225 G. mbp:meGFP expressing oligodendrocytes (top) and mbp:meGFP-calpastatin (bottom) at 4 dpf. Scale  
226 bar= 10µm. Quantitation in 2J.

227 H. Myelin sheath number per oligodendrocyte in DMSO and PD150606 treated animals (n=18 OLs from  
228 18 DMSO-treated animals; n= 33 OLs from 33 PD150606-treated animals; Graph shows mean and SD.  
229 Two-tailed t-test, p=0.006).

230 I. Rate of myelin sheath retraction per hour in DMSO and PD150606 treated animals as analysed by  
231 time-lapse microscopy. (n=14 OLs from 14 DMSO-treated animals and 34 OLs from 34 PD150606-  
232 treated animals. Graph shows mean and SD. Two-tailed t-test, p=0.013).

233 J. Myelin sheath number per mbp:meGFP and mbp:meGFP-calpastatin expressing oligodendrocytes at  
234 4 dpf. (n=31 OLs in 22 mbp:meGFP control animals, and n=29 OLs in 23 mbp:meGFP-calpastatin  
235 animals. Graph shows mean and SD. Two-tailed t-test, p=0.0043).

236

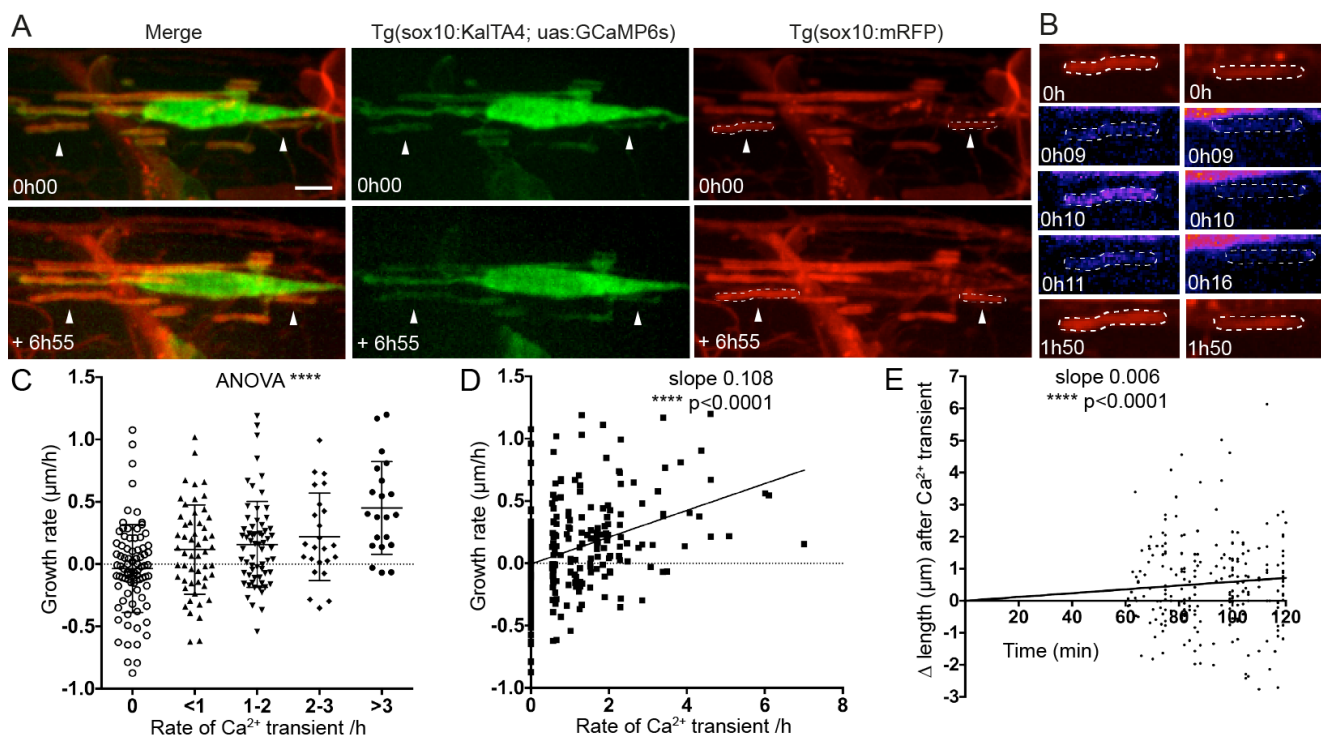


**Figure 3.  $\text{Ca}^{2+}$  transient frequency correlates with sheath elongation**

A. Images of a GCaMP6s expressing oligodendrocyte in a Tg(sox10:mRFP) background allows analysis of the growth and  $\text{Ca}^{2+}$  activity of individual isolated myelin sheaths, e.g. arrowheads over time. Top panels show initial time-point and bottom the same cell at the end of the movie almost 7 hours later. Scale bar=  $5\mu\text{m}$ .

B. Myelin sheaths indicated by arrowheads in A are outlined by ROIs and imaged over time. Note the  $\text{Ca}^{2+}$  transient at 0h 10 time-point in the sheath in the left column subsequently elongates.

C. Growth rate of myelin sheaths ( $\mu\text{m/h}$ ) related to number of  $\text{Ca}^{2+}$  transients per hour. (ANOVA  $p < 0.0001$ ,  $F = 9.225$ . Two-tailed unpaired t-test, 0 vs  $>3$  transients/h  $p < 0.0001$ , 0 vs 2-3 transients/h  $p = 0.0024$ , 0 vs 1-2 transients/h  $p = 0.0011$ , 0 vs  $<1$  transient/h  $p = 0.0162$ ,  $<1$  vs  $>3$  transients/h  $p = 0.0006$ , 1-2 vs  $>3$  transients/h  $p = 0.0014$ , 2-3 vs  $>3$  transients/h  $p = 0.0376$ ; 0 transient/h  $n = 82$  sheaths from 17 animals,  $<1$  transient/h  $n = 53$  from 16 animals, 1-2 transients/h  $n = 64$  sheaths from 17 animals, 2-3 transients/h  $n = 24$  sheaths from 11 animals,  $>3$  transients/h  $n = 21$  sheaths from 11 animals). Graph indicates means and standard deviations.

D. Scatterplot analysis of growth rate of myelin sheaths ( $\mu\text{m/h}$ ) related to number of  $\text{Ca}^{2+}$  transients per hour (Slope= 0.108. Pearson's Correlation Test,  $p < 0.0001$ ,  $n = 244$  sheaths).

E. Change in sheath length over time following 324  $\text{Ca}^{2+}$  transients, with the time of all transients set as time 0 (slope 0.006, Linear Regression test,  $p < 0.0001$ ).

## 259 **Online Methods**

### 260 **Zebrafish husbandry**

261 All animal studies were carried out with approval from the UK Home Office and according to its  
262 regulations, under project licenses 60/ 8436 and 70/8436. The project was approved by the University  
263 of Edinburgh Institutional Animal Care and Use Committee. We used zebrafish (*Danio rerio*) only, and  
264 the following transgenic lines in this study:  $\text{tg}(\text{sox10}(7.2):\text{KalTA4GI})^{21}$ ,  $\text{tg}(\text{UAS:mem-GFP})$ ,  
265  $\text{tg}(\text{uas:GCaMP6s})^{13}$  and  $\text{tg}(\text{sox10:mRFP})^{22}$ . All  $\text{Ca}^{2+}$  imaging was carried out in the nacre background<sup>23</sup>,  
266 which lack melanocytes.

### 267 **Image acquisition**

268 We combined stable transgenic zebrafish  $\text{Tg}(\text{sox10:KalTA4})$ , which drives gene expression in the  
269 oligodendrocyte lineage, with  $\text{Tg}(\text{uas:GCaMP6s})$  that expresses the genetically encoded calcium  
270 indicator GCaMP6s under the control of 14X repetitive Upstream Activator Sequences (uas), the nacre  
271 homozygous mutant line that lacks melanocytes, and also  $\text{Tg}(\text{sox10:mRFP})$  which drives membrane  
272 localised RFP expression in the myelinating oligodendrocyte lineage. The combination of  
273  $\text{Tg}(\text{sox10:KalTA4})$  and  $\text{Tg}(\text{uas:GCaMP6s})$  leads to mosaic expression of GCaMP6s in isolated cells of the  
274 oligodendrocyte lineage in the CNS.

275 Prior to imaging, larvae were screened for the expression of GCaMP6s in isolated oligodendrocytes in  
276 the dorsal spinal cord at 3-4 days post fertilisation (dpf). Selected larvae were paralysed using the  
277 Neuromuscular Junction (NMJ) blocking nicotinic receptor antagonist pancuronium bromide (Sigma,  
278 P1918), which was dissolved in embryo medium (0.15-0.3mg/ml). Larvae were then embedded in 1.3%  
279 agarose for imaging. Imaging was carry out on an Olympus Revolution XDi spinning disk confocal  
280 microscope using a 1.2 NA 60X water immersion objective, plus a camera zoom of 2X, giving an X-Y  
281 image area of  $117 \times 117 \mu\text{m}$  and acquisition at  $512 \times 512$  pixels. Larvae were maintained at  $28^\circ\text{C}$  in  
282 temperature controlled chamber (Okolab). Images were acquired using the iQ3 software (Andor) and  
283 iXon EMCCD Ultra 897 camera.

284 For initial 2D characterisation of calcium transient kinetics,  $\text{Tg}(\text{sox10:KalTA4}, \text{uas:GCaMP6s})$ ,  
285  $\text{Tg}(\text{sox10:mRFP})$  larva were time-lapse imaged for periods of 10-30 min with 100ms exposure time, and  
286 150-250ms intervals, reflecting imaging in one (GCaMP6s) or two (GCaMP6s and mRFP) channels, for  
287 a final rate of 4-6.66 Hz (final rates also incorporate camera integration times).

288 To investigate how  $\text{Ca}^{2+}$  activity related to cell fate,  $\text{Tg}(\text{sox10:KalTA4}, \text{uas:GCaMP6s}, \text{sox10:mRFP})$ ,  
289  $\text{nacre}^{-/-}$  larva were imaged every 60-120 min as follows. First, one high-resolution 3D  $29 \mu\text{m}$  deep  
290 (average  $\pm 2 \mu\text{m}$ ) z-stack of both RFP and GCaMP6s expression was acquired at 100ms exposure, 4x

291 averaging, and z-intervals between optical slices of 0.33 $\mu$ m. Immediately thereafter, 3D time-lapse  
292 images of GCaMP6s expression alone were acquired of the same 29 $\mu$ m ( $\pm$ 2 $\mu$ m) volume, at 100ms  
293 exposure (no averaging), and z step of 1.3 $\mu$ m. The time interval between consecutive z-stacks in the  
294 time-lapse was 2.538s ( $\pm$ 0.264s), including z-positioning and camera integration times. Absolute values  
295 of imaging parameters were incorporated into analyses of all individual Ca<sup>2+</sup> transients and time-lapse  
296 data.

297

## 298 **Image analysis**

299 2D time-lapse imaging data were analysed using Fiji. To correct for sample drift throughout the movie  
300 we used the “Image stabilizer registration” Fiji plugin (Kang Li). Because of the very sparse labelling of  
301 individual GCaMP6s expressing oligodendrocytes it is possible to identify Ca<sup>2+</sup> transients by manual  
302 inspection of time-lapse series. Regions of interest are then applied around all myelin sheaths and also  
303 in a separate area with no GCaMP6s expression, which represents background. Then fluorescent  
304 intensity measurements are extracted from both ROIs and imported into Excel. To measure  $\Delta F/F_0$  we  
305 apply the following formula:  $\Delta F/F_0 = (F(t) - F(0)) / (F(0) - F(\text{background}))$  where  $F(t)$  is the fluorescence  
306 intensity in the ROI in which the Ca<sup>2+</sup> transient was observed at time (t),  $F(0)$  the average fluorescence  
307 intensity of the first 4 frames of the movie in the same ROI and  $F(\text{background})$  the fluorescence  
308 intensity of the background ROI at time (t). See Supplementary Figure 1 for overview. This  $\Delta F/F_0$   
309 information and corresponding image acquisition parameters are imported into pClamp (Molecular  
310 Devices) for detailed analyses of the duration and amplitude of individual Ca<sup>2+</sup> transients.

311 For 3D time-lapse imaging data, maximum intensity projections of the individual time-points from 3D  
312 time-lapse data were made using Fiji and the image stabilizer Fiji plugin was again run to account for  
313 drift. In parallel 3D datasets were registered using the “Descriptor-based series registration (2d/3d+t)”  
314 Fiji plugin, after which maximum intensity projections are made and Ca<sup>2+</sup> transients identified  
315 manually. Ca<sup>2+</sup> transients were then identified manually. Only Ca<sup>2+</sup> transients identified following both  
316 modes of image processing were considered as valid. All myelin sheaths without overlapping structures  
317 in the X-Y or Z planes were analysed. Regions of interest are then applied around all myelin sheaths  
318 and corresponding background, as above. In addition, the ROI with the candidate Ca<sup>2+</sup> transient was  
319 moved to an immediately adjacent region in order to rule out the possibility that any, very infrequent,  
320 general increase in background fluorescence in the region could identify a spurious transient. Key  
321 parameters for analysis of 3D time-lapse datasets were extracted from the iQ3 metadata files using a  
322 custom-written Fiji macro written by Dr. Bertrand Vernay, University of Edinburgh. These parameters

323 were then imported into Microsoft Excel for analysis. All  $\text{Ca}^{2+}$  transients were identified by  $\Delta F/F(0)$  as  
324 above and analysed using pClamp.

325

326 To measure myelin sheath length, we used the 3D high-resolution single time z-stack datasets acquired  
327 before each period of GCaMP6s time-lapse imaging. The expression of GCaMP6s allowed identification  
328 of individual myelin sheaths and the membrane localised mRFP in the same sheaths allowed more  
329 accurate measurement of length.

330

### 331 **Calpain inhibitor treatment and analysis**

332 The calpain inhibitor PD150606 (Tocris) was applied in solution from 50 $\mu\text{M}$  -75 $\mu\text{M}$  with 1% DMSO to  
333 embryos from 2-4 dpf and vehicle alone applied to controls. The morphology of myelinating  
334 oligodendrocytes was assessed as previously by imaging individual oligodendrocytes expressing the  
335 mbp:mCherry-CAAX reporter<sup>6</sup>. Images of individual myelinating oligodendrocytes were taken on a  
336 Zeiss 880 with Airyscan, in animals immobilized using 1.3% Low melting point agarose with 0.03%  
337 Tricaine in embryo medium. Individual myelin sheaths were identified in 3D z-stacks and measured  
338 using Fiji. Time-lapse analyses were carried out using tg(sox10(7.2):KalTA4GI), tg(UAS:mem-GFP),  
339 animals, which were imaged on a Zeiss 880 Airyscan in Fast Mode and with a piezo z-drive to allow  
340 rapid acquisition of confocal z-stacks. Z-stack images were collected every 5 minutes for a 15 hour  
341 period from 81-96 hpf.

342

### 343 **Cell-type specific expression of calpastatin in myelinating oligodendrocytes**

344 In order to disrupt calpain function in a cell type specific manner, we chose to express the endogenous  
345 inhibitor of calpain, calpastatin<sup>24</sup>, in myelinating oligodendrocytes. We first cloned zebrafish  
346 calpastatin. To do so, we extracted mRNA from whole zebrafish embryos at 3 and 4 dpf, generated  
347 cDNA and amplified calpastatin using the following primers castF: 5'- ATGGCGTACGCAATGTATTGG -3';  
348 castR: 5'-TTATCTTTTTCCAGCCTTTGTGG-3' and high fidelity Phusion polymerase (Thermo Fisher). We  
349 cloned cast fragments into pCR<sup>TM</sup>-Blunt II-TOPO<sup>TM</sup> (Thermo Fisher) and Sanger sequenced clones  
350 (Source Bioscience). We subcloned multiple cast mRNA variants into pCS2+ and generated synthetic  
351 mRNA, which we injected into animals at the one cell stage to identify full-length version that lead to  
352 an increase in myelin sheath number per oligodendrocyte in the dorsal spinal cord (Supplementary Fig.  
353 5 and data not shown). We next generated a p3E vector in which full length cast was flanked by p2A  
354 and a SV40 polyA sequences. We then generated a pME vector with the Fyn myristoylation domain  
355 added to GFP, by amplifying GFP from pCS2+eGFP and adding the myristoylation sequence using the

356 following primer meGFPF 5'-ATGGGCTGTGTGCAATGTAAGGATAAAGAAGCAACAAAAGTACG-3.' To  
357 generate a construct for cell type specific expression of meGFP-pA or meGFP-2A-cast-pA we  
358 recombined the previously described p5E-mbp plasmid containing zebrafish myelin basic protein  
359 regulatory sequence<sup>25</sup>, with the pME-meGFP and p3E-pA or with the pME-meGFP and p3E-2A-cast-pA.  
360 mbp:meGFP-pA (5pg) or mbp:meGFP-2A-cast-p2A (10pg) plasmids were injected into zebrafish at the  
361 1-2 cell stage together with 25pg tol2 mRNA<sup>26</sup>. Individual oligodendrocytes were imaged at 4dpf using  
362 meGFP on a Zeiss 880 Airyscan confocal microscope in Fast Mode.

363

#### 364 **Statistics and reproducibility**

365 All data are shown as mean  $\pm$  standard deviation or median with 1<sup>st</sup> and 3<sup>rd</sup> quartiles as indicated.

366 All the statistical tests were carry out using GraphPad (Prism 6 or 7). Power calculations were calculated  
367 using Statemate 2 to determine for Ca2+ imaging analyses, and investigations of the role of calpain  
368 signalling in myelination. All analyses had a power >80%. Randomisation of imaging and analyses was  
369 not carried out on animals whose myelin sheaths were Ca2+ imaged, as all are wildtype. For chemical  
370 and genetic manipulations of calpain function, zebrafish embryos for both experimental and control  
371 conditions derived from the same clutch (per experiment). For time-lapse analyses of chemical  
372 inhibitor treated animals, control and experimental animals were imaged separately for technical  
373 reasons. Embryos were grown up in the same incubator and the same conditions prior to analyses, all  
374 live imaging. During live imaging analyses, experimental and control animals were imaged in an  
375 alternating pattern (per experiment) to ensure no confounding effects of stage of development  
376 between groups. The analysis of all experimental findings were carried out blinded and image data was  
377 randomised using a custom-made script.

378 The data shown in Supplementary Figure 1 is representative of 20 myelin sheaths imaged in 12 animals  
379 over 4 separate experimental sessions.

380 The data shown in Figure 1A-E and Supplementary Figure 2 are representative of 40 oligodendrocytes  
381 imaged in 40 animals over 25 separate occasions.

382 The images analysed and data presented in Figures 1G-K, 2A-D and Figure 3 are representative of 18  
383 cells imaged over 9 separate experimental sessions.

384 The images analysed and data presented in Figure 2E,H are representative of 4 experimental sessions.

385 The images analysed and data presented in Figure 2G,J are representative of 4 experimental sessions.

386 The images analysed and data presented in Figure 2F,I are representative of 6 experimental sessions.

387 Data were tested for normality by the D'Agostino & Pearson omnibus normality test. Normal  
388 distributed data were tested as appropriate by two-tailed student's t-test unpaired (equal variance was  
389 tested using the F test) or two-tailed one-way ANOVA (equal variance was tested using the Brown-  
390 Forsythe test). Non-normally distributed data were tested by a two-tailed Mann-Whitney tests. The  
391 Pearson's correlation test was used to test the correlation in Fig.1J and Fig. 3D. Linear regression  
392 analyses were used to test whether the slopes differed significantly from zero in Fig. 3E. Throughout  
393 all analyses \* p<0.05, \*\*p<0.01, \*\*\*p<0.001, \*\*\*\*p<0.0001.

394 Please see Life Sciences Reporting Summary for further details on experimental design.

395 Data and code availability

396 Transgenic constructs and transgenic zebrafish lines will be available upon request. The data that  
397 support the findings of this study are available from the corresponding author upon reasonable  
398 request. Custom written code for analyses of Ca<sup>2+</sup> imaging data are specific to the imaging platform,  
399 but details are available upon request. Custom written codes for blinding of image analyses are  
400 available upon request.

401

402 **Supplementary References (Online Methods)**

- 403 21. Almeida, R.G. & Lyons, D.A. *Zebrafish* **12**, 377–386 (2015).  
404 22. Kirby, B.B. et al. *Nat Neurosci* **9**, 1506–1511 (2006).  
405 23. White, R.M. et al. *Cell Stem Cell* **2**, 183–189 (2008).  
406 24. Kiss, R., Kovács, D., Tompa, P. & Perczel, A. *Biochemistry* **47**, 6936–6945 (2008).  
407 25. Almeida, R.G., Czopka, T., Ffrench-Constant, C. & Lyons, D.A. *Development* **138**, 4443–4450  
408 (2011).  
409 26. Kwan, K.M. et al. *Dev. Dyn.* **236**, 3088–3099 (2007).  
410

411

412